



## **GAS AND AEROSOL LEAKAGE RATE THROUGH REINFORCED CONCRETE SHEAR WALLS: EXPERIMENTAL STUDY**

**Charles H. HAMILTON<sup>1</sup>, Tara C. HUTCHINSON<sup>1</sup>, Gerard C. PARDOEN<sup>1</sup>, Michael W.  
SALMON<sup>2</sup>, and Ting WANG<sup>1</sup>**

### **SUMMARY**

Many radioactive material storage facilities in the United States Department of Energy inventory rely on unlined reinforced concrete walls as tertiary containment barriers. Following damage to the structure arising from seismic or other severe loading, substantial residual cracking may be present, especially in stiff lateral force-resisting elements such as concrete shear walls. It is important that engineers evaluating the functionality of such structures have experimentally-verified guidance on the probable level of containment of contaminants given the damaged state of the facilities.

Two major forms of contaminant release are of concern in the case of evaluating containment failure: gases and particles. In order to address these concerns, an experimental program was undertaken to measure the variation in gas permeability and aerosolized particle filtration efficiency with increasing levels of imposed damage. A reduced-scale reinforced concrete shear wall specimen was subjected to sequentially-phased lateral loading cycles up to the nominal code force capacity, and then subjected to sequentially-phased lateral drift cycles beyond nominal code capacity. At each load and drift level, the specimen's effective intrinsic gas permeability and aerosol filtration efficiency were measured using flow measurements and laser aerosol spectroscopy, respectively. These measurements were correlated with engineering demand parameters including lateral drift and fraction of nominal code capacity. It was determined that at 100 percent of the nominal code capacity, the shear wall maintained a minimum 99.5 percent aerosol filtration efficiency for particle diameters from 0.065 $\mu\text{m}$  to 1 $\mu\text{m}$ , and an effective intrinsic permeability of  $3.1 \times 10^{-11} \text{ in}^2$ . Permeability increased by a factor of 27 from the undamaged condition until loading exceeded 50 percent of the nominal capacity, and showed essentially linear variation with increased load thereafter. These data provide a basis for comparison with numerical models used to predict gas leakage rates, which are presented in a companion paper. [1]

---

<sup>1</sup> Post-doctoral Research Fellow and Lecturer, Asst. Professor, Professor, and Doctoral Candidate, respectively. Dept. of Civil and Environmental Engineering, University of California, Irvine, 92697-2175

<sup>2</sup> Civil/Structural/Architectural Team Leader, Facilities and Waste Operations, Design Engineering, Los Alamos National Laboratory, MS 702 Los Alamos, NM 87545

## INTRODUCTION

Many nations have stockpiles of radioactive materials, either as fissile material or as waste products which have been placed in storage. In many cases, these materials are stored in facilities where unlined reinforced concrete walls serve as a tertiary containment barrier. The U.S. Department of Energy alone has hundreds of such facilities. Given the potential for contamination posed if these walls should fail to perform effectively as containment barriers, the containment capacity of these walls is of utmost importance.

Concrete walls can permit radioactive materials to escape through a variety of mechanisms. High-level radioactive materials may emit radiation directly as  $\alpha$  or  $\beta$  particles, which can be readily contained by thin layers of shielding, or  $\gamma$  rays, which are obstructed only by the placement of shielding composed of high-density cementitious materials, or other dense barriers. Lower-level radiation-contaminated materials, as are encountered in most waste products, are typically considered radiation hazards only through transport of the radioactive gases or particulates themselves, rather than through the direct release of radiation. Such transport typically occurs either through natural or induced voids in the concrete, and is of primary interest in this study.

Induced voids are most commonly the result of structural damage. Since lateral deformation is the most likely cause of significant damage to reinforced concrete shear walls, this program explored the effects of increasing lateral demands on intrinsic permeability and aerosol filtration efficiency, two major indicators of containment efficacy. These results were compared against the baseline undamaged condition to evaluate the degradation of the wall's gas and aerosol containment capacity.

## EXPERIMENTAL PROCEDURES

### Test specimen

The reinforced concrete wall test specimen was designed to be comparable to a specific facility in the U.S. Department of Energy inventory, which is believed to be representative of many such structures. The facility was initially considered in a series of studies conducted by Girrens [3] specifically for the task of ascertaining whether or not the facility met design guidelines at several limit states specific to the facility itself. As a result, the focus of those studies was not on developing or assessing models for gas or aerosol permeability behavior of general reinforced concrete walls. In contrast, an important component of the current research has been establishing the limits of extant models for gas and aerosol permeability.

The wall specimen was fabricated from a concrete mix using 0.75 in crushed rock aggregate and having a 28-day nominal compressive strength of 4 ksi. The w/c ratio was 0.38, with admixture dosages of high-range water-reducer (WRDA-79) at 148 mL/Cwt and an air-entraining agent (Microair) at 14.8 mL/Cwt. The specimen configuration was an H-shaped wall section in which the surface of interest was the "web" of the section. The flanges served to enclose a volume for the pressurized permeability testing discussed in the following sections. The wall was 6 in thick. The web section had a surface area 24 in tall by 36 in long. The flanges extended a distance of 13 in from the face of the web, enclosing a volume of just over 6.5 ft<sup>3</sup>. The point of load application, h, was 48 in above the point of base of the wall.

The wall itself was reinforced with CRSI D3 deformed steel reinforcing bars with a nominal yield strength of 60 ksi. These bars were placed in offset mats on each face of the wall, with vertical bars placed on 3 in centers and horizontal bars placed at 5 in centers. One inch of minimum clear cover was provided to the reinforcing steel on all surfaces. Refer to Figure 1 for a schematic of the wall section. An overall view of the test configuration is shown in Figure 2.

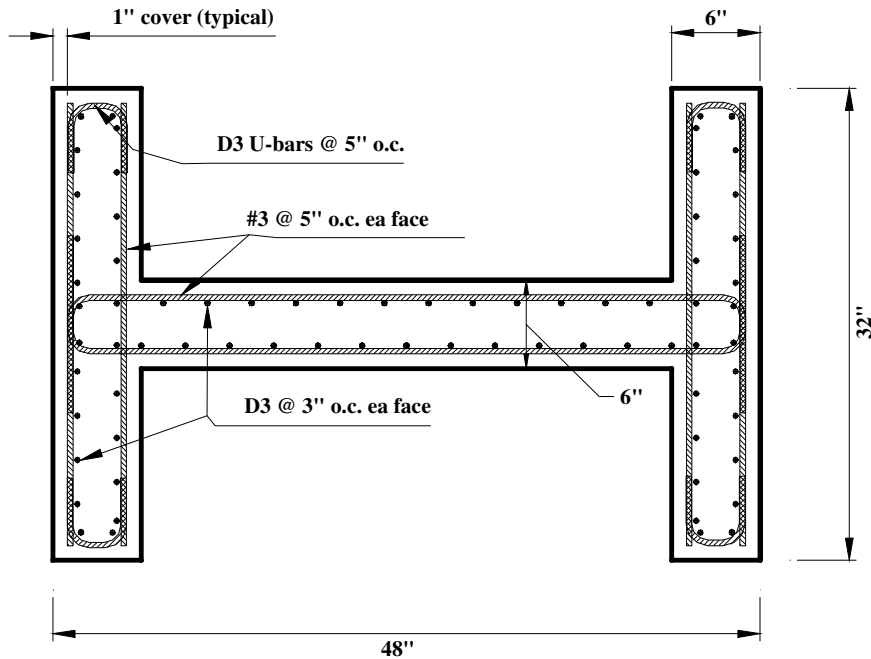


**Figure 1 Section through specimen wall**

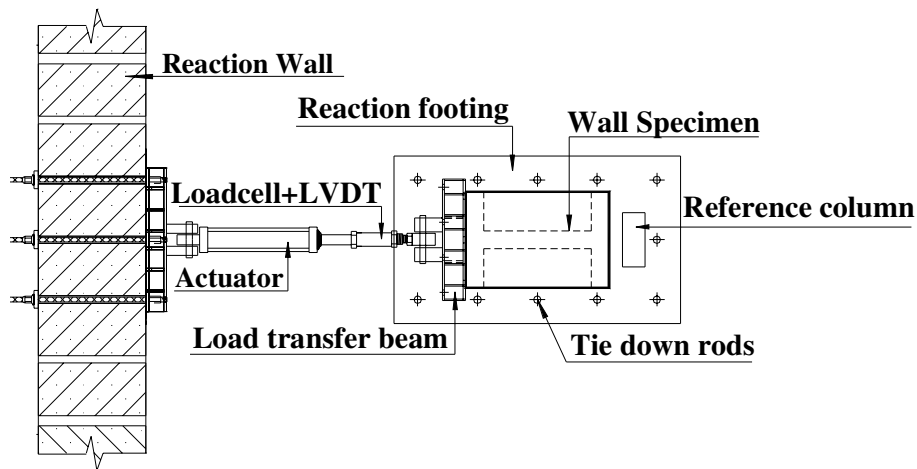


**Figure 2 Lateral testing configuration**

The techniques used to determine the permeability of the specimen require a known flow surface. As a result, it was necessary to make all other potential paths for flow impermeable. Two coats of two-part epoxy paint were applied to all exterior surfaces of the specimen, and to the interior surfaces of the flanges, roof, and floor of the pressure chambers of the specimen. This paint prevented gas flow from inside the pressurized volume except through the uncoated web of the flanged wall.

To permit pressurization of the two faces of the specimen, two aluminum cover plates were fabricated. These plates were attached to the concrete wall specimen using cast-in-place J-bolts embedded around the

perimeter of the specimen opening. A Buna-N O-ring was used to ensure a pressure-tight fit between the concrete and the aluminum plates. Leak tightness was verified using helium leak detection to ensure that all measured flow was through the uncoated concrete web.

### Lateral loading protocol

The wall specimen was subjected to in-plane reversed-cyclic lateral loading using servo-controlled actuators. Lateral loading rates were quasi-static (5 minutes per cycle) to ensure that there were no strain-rate effects and allow specimen observation during loading. The loading protocol included three fully-reversed cycles to each of four lateral load levels:  $0.30\phi V_n$ ,  $0.50\phi V_n$ ,  $0.75\phi V_n$ , and  $1.00\phi V_n$ , where  $\phi V_n$  is the lateral load capacity of the wall as defined by ACI 318-02. [2] Each loading phase terminated at zero lateral load. The loading protocol shown in Figure 3 represents the load applied at the nominal height of the wall, being the centerline of the top plate of the specimen. The circles indicate points at which the containment capacity was measured.

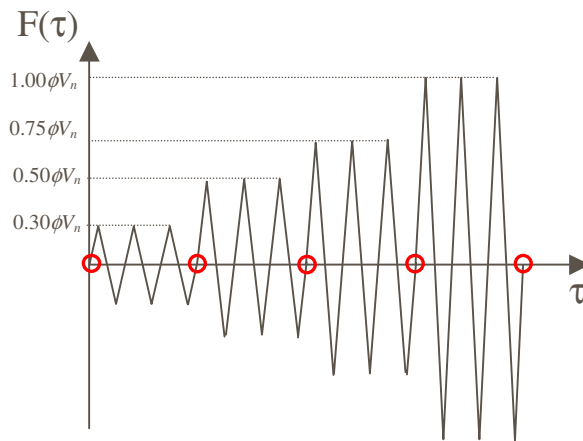


Figure 3 Lateral loading protocol

### Permeability measurement techniques

For both gas and aerosol permeability, the temperature and absolute pressure on each side of the concrete wall were continuously recorded using a digital data acquisition system. The following sections describe the techniques for measuring the gas and aerosol permeability of the specimen.

#### *Gas permeability*

Two techniques were used to measure the gas permeability of the uncoated concrete wall. The first technique was simply to pressurize one side of the wall, henceforth the “upstream” side, and permit the pressure to decay by permeation through the uncoated concrete wall to the “downstream” side, which was maintained at atmospheric pressure. This technique is termed the pressure-decay method (PDM). The second technique employed was to establish a steady-state flow across the wall at a given differential pressure, and measure the required inlet gas flow rate to maintain this pressure. This technique is termed the steady-state flow method (SFM). PDM simulates a pressure gradient which is transient in comparison with the time needed to establish steady-state flow. SFM simulates a prolonged period of differential pressure which allows the development of steady-state or near-steady-state flow.

Using PDM, it is possible to extract the intrinsic permeability for the concrete shear wall [3] based on a Darcy's Law derivation. This relationship can be used to generate an explicit expression for the intrinsic permeability of the concrete shear wall:

$$k = \frac{2\mu t_w V T_m}{A \cdot \Delta t (P_m^2 - P_{atm}^2)} \left( \frac{P_t}{T_t} - \frac{P_{t+\Delta t}}{T_{t+\Delta t}} \right) \quad (1)$$

where upstream temperature (T) and all pressures are measured in absolute scale.  $P_t$  represents the pressure in the upstream chamber at the beginning of the decay period,  $\Delta t$ , and  $P_{t+\Delta t}$  is the pressure at its end.  $P_m$  is the mean chamber pressure during the decay period, and  $P_{atm}$  is the mean atmospheric pressure during the decay period. A,  $t_w$ , and V denote the wall surface area, wall thickness, and upstream enclosed volume, respectively. This relationship was used to obtain the values of intrinsic permeability reported in Table 1.

The dynamic viscosity of air,  $\mu$ , was taken to vary according to the relation provided by Girrens [3]:

$$\mu = (5.672 \times 10^{-5} \cdot T + 0.0338) \times 10^{-5} \text{ lbf} \cdot \text{s} / \text{ft}^2 \quad (2)$$

with the temperature, T, in degrees Fahrenheit.

Using SFM with a differential pressure across the wall of  $\Delta p$ , the intrinsic permeability can be computed as

$$k = \frac{Q \cdot \mu \cdot t_w}{\Delta p \cdot A} \quad (3)$$

The volume flow rate of the air needed to maintain a constant pressure in the “upstream” side, Q, was monitored using an assembly (Figure 4) of individually-valved laminar flow elements (LFE). Each LFE produces a pressure drop due to flow constriction. The magnitude of this pressure drop, which was monitored electronically with the other test variables, is proportional to the flow velocity across the LFE, as indicated by Bernoulli's Law. Based on these calibrated LFEs, the volume flow term in Equation (3) can be determined. Equation (3) was used to obtain the values reported in Table 2.

#### *Aerosol filtration efficiency*

To assess the aerosol filtration efficiency of the shear wall, a polydisperse aerosol of dioctyl sebacate (DOS) was injected into the upstream enclosed volume under conditions of steady state flow. The aerosol in the volume was measured for particle size distribution and particle count within the distribution using a laser aerosol spectrometer (LAS). Since the concentration of the particulate in the upstream volume, termed the challenge concentration, was very high in comparison with the saturation level of the LAS, it was necessary to dilute the sampled gas. This was achieved using a capillary-type aerosol diluter. The sampled gas was then reintroduced into the upstream volume to preserve volume and pressure. The apparatus for conducting this test is shown in Figure 5.

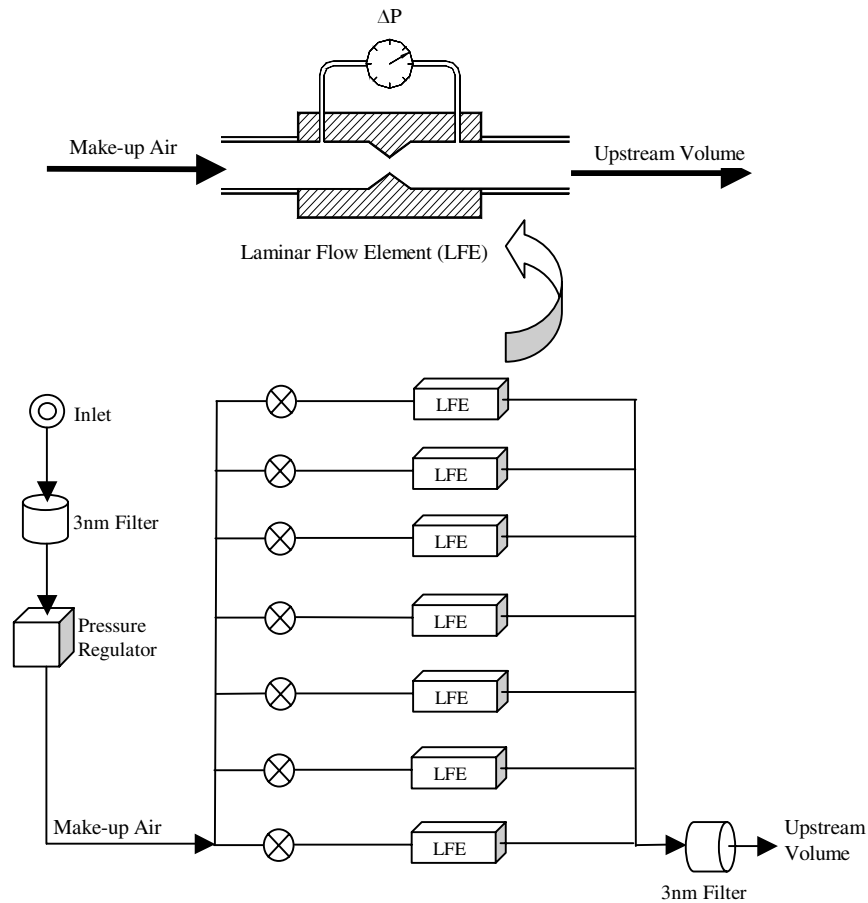


**Figure 4 Gas flow measurement manifold**

Based on the measured aerosol distribution and particle count, it is possible to obtain the aerosol challenge concentration spectrum by sampling the upstream volume through a diluter which has been adjusted to provide aerosol concentrations within the range of the LAS. The measured concentration at each particle size is then corrected for the dilution ratio. Similarly, for measurements of the aerosol penetration spectrum, the LAS was used to collect a sample from the downstream volume. This measurement, however, was not diluted as the expected concentration was quite low in comparison with the challenge concentration. The apparatus for measuring aerosol penetration is shown in Figure 6.

For both the challenge and penetration concentration spectra, it was necessary to obtain a background airborne particle spectrum. This was done by using the procedure for obtaining the penetration spectrum. That is, no dilution of the measured volume was made. In order to minimize the background spectrum, each volume to be enclosed was wiped-out three times immediately prior to attaching the cover plates using acetone and lint-free rags. This removed the majority of the dust and residual DOS present on the surface of the specimen. Circulation of clean air through the specimen during the establishment of steady-state flow also reduced the background airborne particle count.

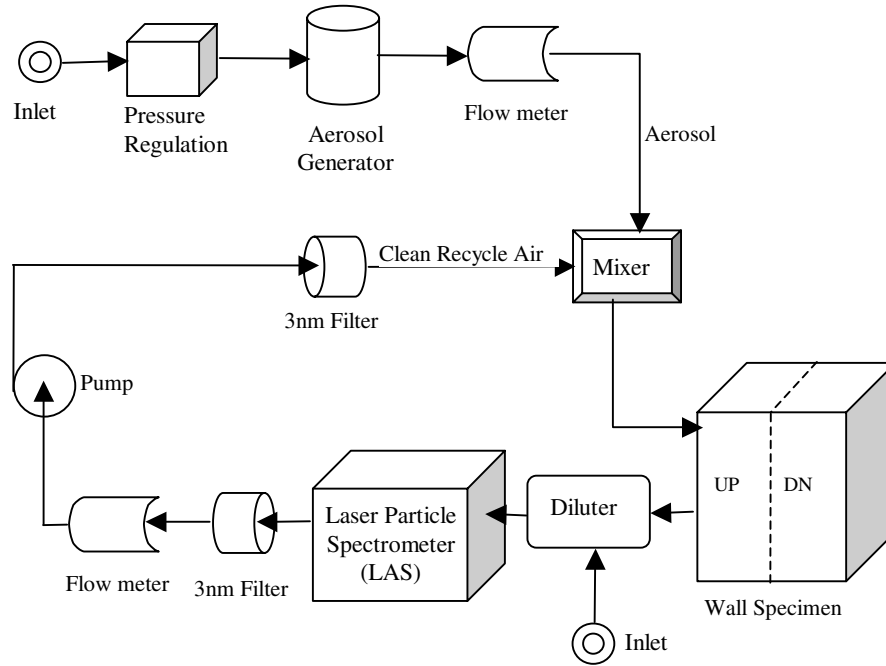


**Figure 5 Upstream aerosol concentration measurement loop**

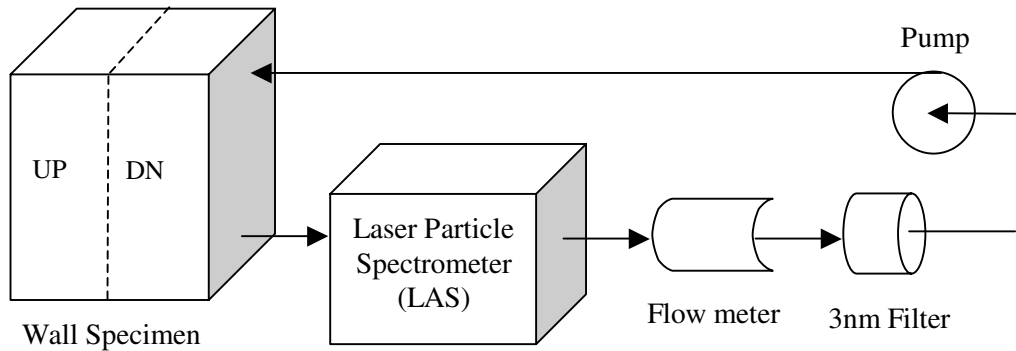


**Figure 6 Downstream aerosol concentration measurement loop**

The aerosol filtration efficiency (AFE), for a given set of measurements was computed by taking the ratio of the penetration spectrum amplitude at any given particle size to the expected spectrum amplitude assuming complete penetration at that particle size. That is, for AFE expressed as a percentage,

$$AFE = \left( 1 - \frac{N_{down} \cdot V_{down}}{N_{up} \cdot Q \cdot \Delta t} \right) \cdot 100 \quad (4)$$

where  $N_{up}$  and  $N_{down}$  denote the upstream and downstream particle concentration, respectively,  $V_{down}$  denotes the downstream enclosed volume,  $Q$  denotes the volumetric flow rate across the wall, and  $\Delta t$  denotes the elapsed time between injection of the aerosol and the measurement.

## DISCUSSION OF RESULTS

### Lateral capacity

As can be observed from Figure 7, the lateral response of the wall specimen was almost fully linear through 50 percent of the nominal lateral load capacity, with secant stiffnesses of 7480 kips/in and 7080 kips/in, respectively, for the first two loading levels. The wall demonstrated significant nonlinear response at  $0.75\phi V_n$ , having a secant stiffness of 6244 kips/in. During cycling to its code design capacity, the wall exhibited pinching of its hysteresis loops typical of shear-dominated response. The secant stiffness at this loading level was 4568 kips/in.

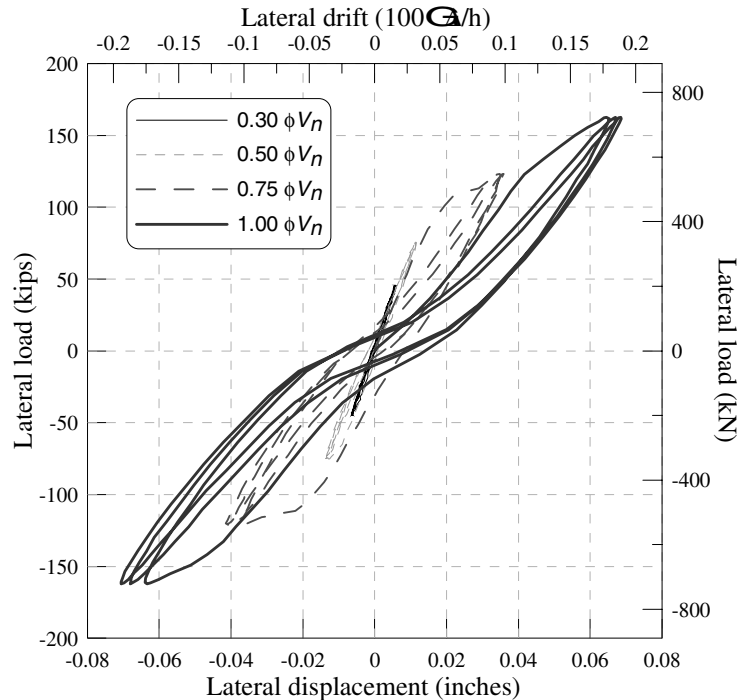


Figure 7 Lateral load-displacement hysteresis response of wall

No visible cracking was observed following the lateral loading cycles to  $0.30\phi V_n$ , and the gas permeability results from this testing level confirm that only minimal sub-visible cracking was present, as is discussed in a subsequent section. No measurable residual displacement was recorded. During the last cycle to 50 percent of the nominal capacity, minor cracking appeared, with typical surface crack widths of  $4\times 10^{-3}$  in to  $12\times 10^{-3}$  in. These cracks closed to become invisible after relief of lateral loading. Residual lateral deformation of approximately  $2\times 10^{-3}$  in was measured after removal of the lateral load. Following cycles to  $0.75\phi V_n$ , inclined cracking parallel to the main diagonals of the wall plane was observed, with significant crack localization in the bottom corners of the wall. Surface crack widths of up to  $79\times 10^{-3}$  in were measured during loading, with only hairline residual cracks following unloading. Residual lateral displacement of  $8\times 10^{-3}$  in was recorded on return to zero load. During the cycles to 100 percent of the nominal lateral capacity, the wall had developed a significant shear mechanism, with inclined shear cracks nearly evenly distributed across the face of the wall. Residual crack widths were greatest – approximately  $8\times 10^{-3}$  in – near the diagonal to which they were parallel, becoming invisible further away. A residual displacement of  $17\times 10^{-3}$  in was recorded.

The lateral load-displacement capacity of the wall is enveloped very accurately by a bilinear model, with a slope change at 0.06 percent drift. This behavior offers the potential to model the structural response of the wall with a simple pushover curve. The advantages of this model are significant, given that nonlinear pushover analysis is gaining acceptance in the design community at a rate substantially greater than that for either linear or nonlinear time history analysis. The ability to assess the performance of a structural element as a containment vessel, using a simple method like pushover analysis to characterize its structural state, puts the application of this information within the realm of techniques commonly accepted by practicing engineers.

### Gas permeability

The intrinsic permeability,  $k$ , was measured using two methods, PDM and SFM, as described in the previous section. Figure 8 shows the influence of initial pressure gradient on the PDM-measured intrinsic permeability after various levels of lateral loading. It can be seen that the intrinsic permeability is essentially constant across initial pressure gradients at levels of lateral load up to  $0.50\phi V_n$ . However, at  $0.75\phi V_n$  and  $1.00\phi V_n$ , substantial scatter is observed in the measurements.

However, the average values,  $\mu_k$ , and coefficients of variation,  $COV_k$ , obtained using the PDM are of the same order of magnitude as those obtained using SFM, as shown in Tables 1 and 2. Figure 9 shows that the intrinsic permeability measured using SFM is relatively independent of pressure gradient for a given lateral load, as indicated by the essentially horizontal least-squares regression lines for each loading level. This is consistent with the relationship among intrinsic permeability, pressure gradient, and volume flow rate shown in Equation (3). The absence of pressure dependence in the intrinsic permeability measured using SFM is demonstrated in Figure 10. Similar measurements can not be made for pressure decay, due to the nature of the test.

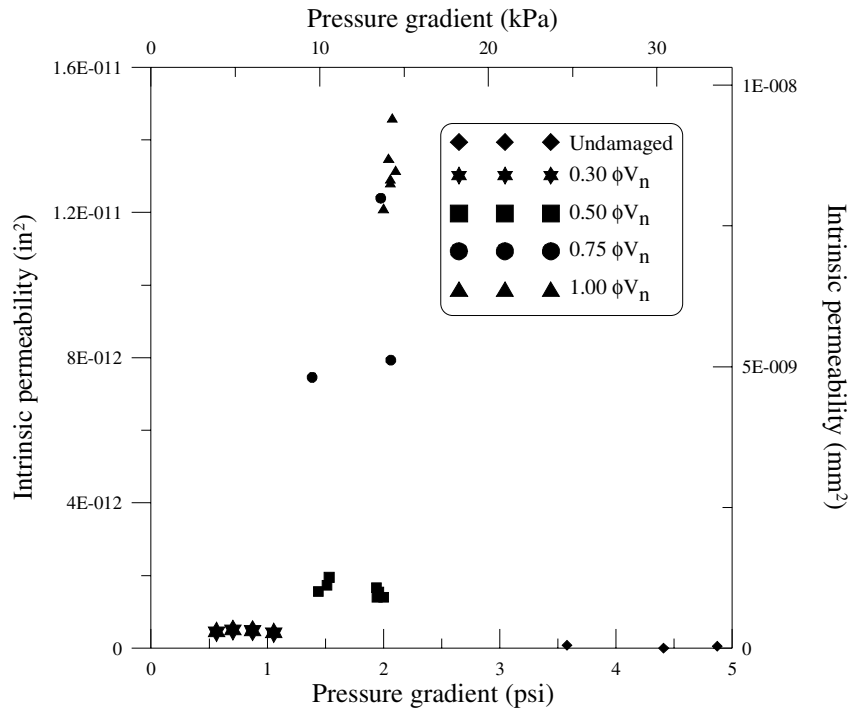


Figure 8 Variation of intrinsic permeability with initial pressure gradient for PDM measurements

**Table 1 PDM permeability measurements**

Peak load	$\mu_k$ ( $10^{-14} \text{ in}^2$ )	$\text{COV}_k$
0	4.61	0.85
$0.30\phi V_n$	46.4	0.07
$0.50\phi V_n$	161	0.12
$0.75\phi V_n$	926	0.29
$1.00\phi V_n$	1320	0.06

**Table 2 SFM permeability measurements**

Peak load	$\mu_k$ ( $10^{-14} \text{ in}^2$ )	$\text{COV}_k$
0	6.89	0.32
$0.30\phi V_n$	34.4	0.09
$0.50\phi V_n$	185	0.14
$0.75\phi V_n$	1630	0.02
$1.00\phi V_n$	3060	0.02

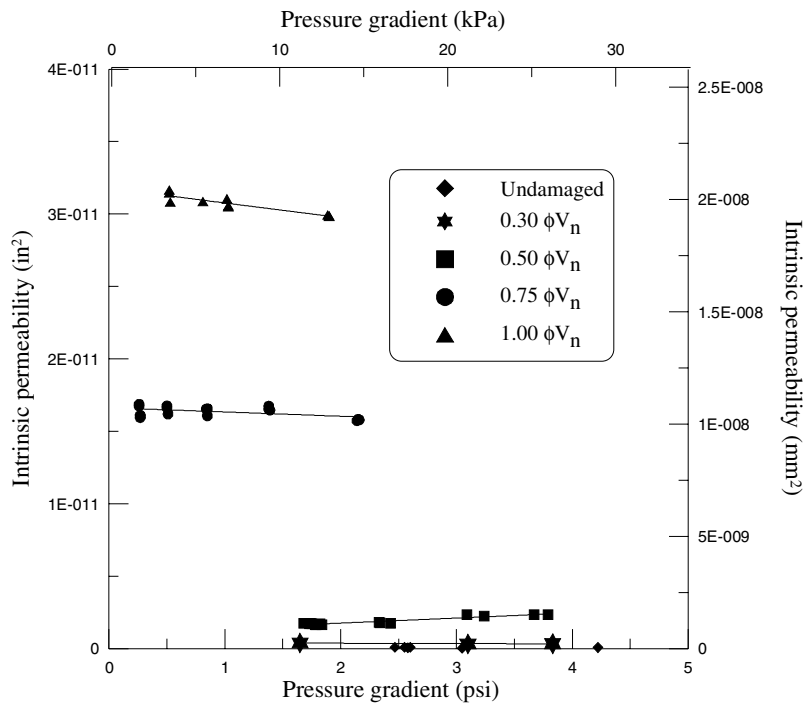


**Figure 9 Variation of intrinsic permeability with pressure gradient for SFM measurements (Solid lines represent least-squares regression)**

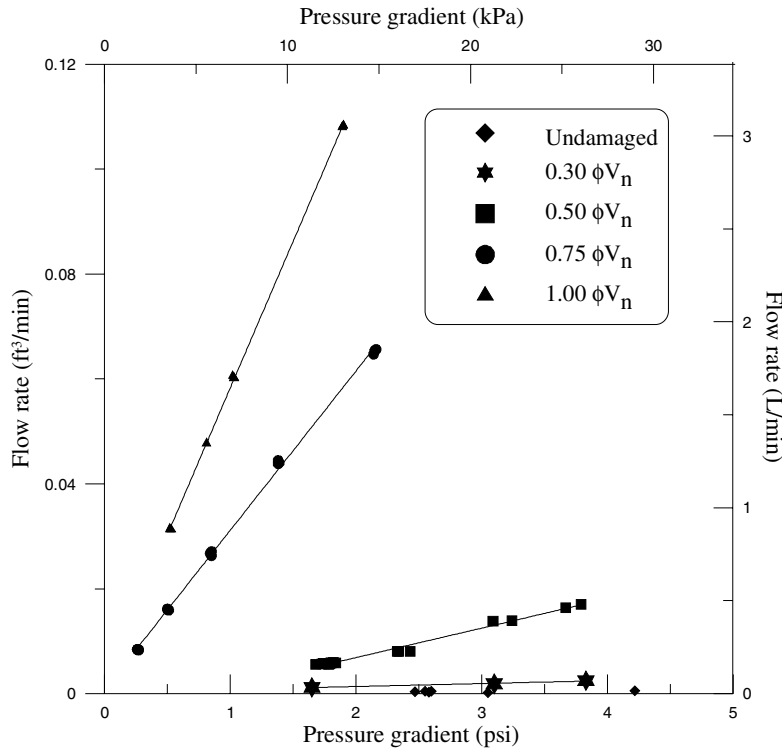


**Figure 10 Variation of volumetric flow rate with pressure gradient for SFM measurements (Solid lines represent least-squares regression)**

It can be observed from Figure 11 that the intrinsic permeability determined using SFM shows two sharp changes in slope at approximately  $0.30\phi V_n$  and  $0.50\phi V_n$ , which correspond to drift ratios of 0.02% and 0.04%, respectively. The first change can be attributed to the initiation of diagonal microcracking, as reported in the discussion of the lateral deformation response. Similarly, the onset of significant nonlinear response occurred during the last cycle to  $0.50\phi V_n$ . The intrinsic permeability has a very low coefficient of variation at each loading increment, as can be seen from the  $\mu \pm \sigma$  bounds superimposed on the plot. This variability increases with increasing lateral load, likely due to the increase in the number of large cracks, which can be expected to impose more random effects on gas flow than would narrower cracks. Figure 12 clearly shows the higher scatter in the PDM measurements, and the influence of this scatter on the observed relationship between intrinsic permeability and damage. The measurements obtained using SFM are taken to be more accurate, given their lower scatter.

There are a number of relationships which can be used to predict the volumetric flow rate of gas through a concrete plate. For example, Fintel [4] asserts that the rate of volume flow per unit area in  $(\text{in}^3/\text{hr})/\text{ft}^2$ , across an undamaged concrete slab of thicknesses between 4 in and 9 in, is approximately 12.5 times the ratio of the differential pressure to the thickness in psi/in. Based on this relationship, the volume flow across the undamaged wall should be approximately  $3 \times 10^{-4} \text{ ft}^3/\text{min}$ . This corresponds to an intrinsic permeability value of  $6.4 \times 10^{-14} \text{ in}^2$  based on Equation (3), assuming air viscosity equal to the average of that for the measurements taken during the undamaged wall tests. Both the predicted volume flow rate and the associated intrinsic permeability are within approximately 15 percent of the measured values. The results of a study by Girrens [3] indicated a mean undamaged intrinsic permeability of  $1.2 \times 10^{-13} \text{ in}^2$ . Their testing to  $0.33\phi V_n$  resulted in an average intrinsic permeability of  $1.1 \times 10^{-13} \text{ in}^2$ , essentially unchanged

from the undamaged state. A single cycle to  $0.5\phi V_n$  increased the effective intrinsic permeability to  $4.7 \times 10^{-12} \text{ in}^2$ , which is approximately three times the value measured in this research, but is of comparable magnitude. However, relative humidity can substantially influence gas permeability, in that lower humidity periods tend to increase measured intrinsic permeability, especially for concrete with low w/c ratios. [5] The relative humidity during the Girrens curing period was typically between 20% and 30%, while that in the present program was typically in the range of 70% to 80%, so it is reasonable to expect greater measured permeabilities in the former case. Since methods predicting flow through cracked concrete elements require data on the crack pattern and crack widths, discussion of these methods is presented in the companion paper [1] addressing numerical simulation.

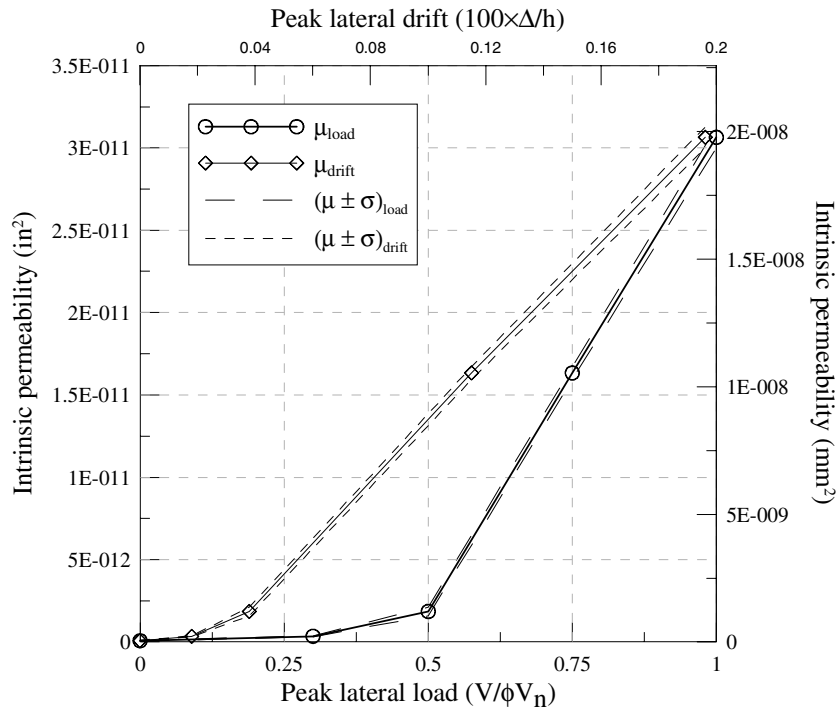


**Figure 11** Variation of SFM intrinsic permeability with peak demand

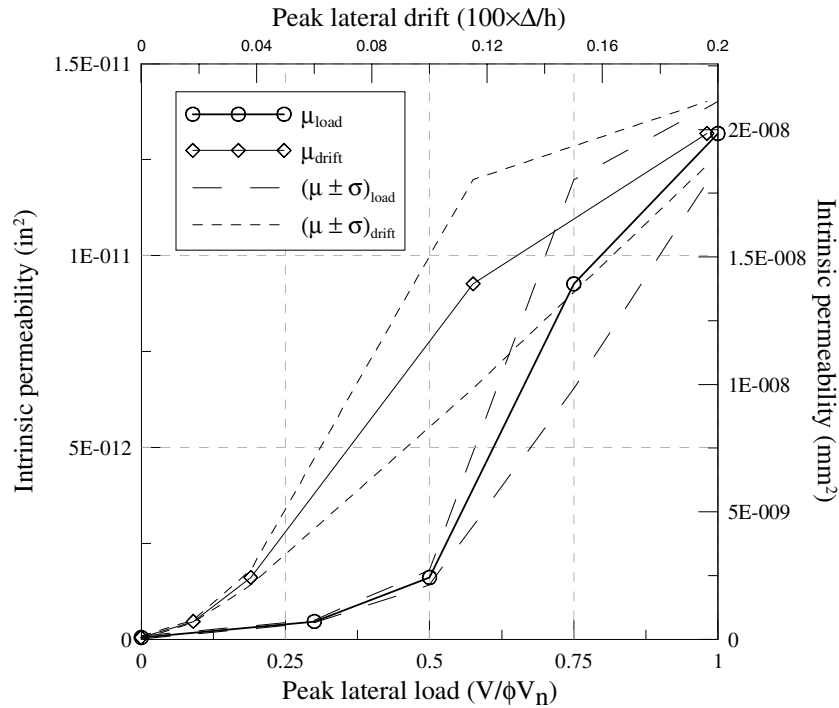


**Figure 12 Variation of PDM intrinsic permeability with peak demand**

### Aerosol filtration efficiency

Very little has been published regarding theoretical relationships for aerosol permeability of uncracked concrete members. The pilot study by Farrar [6] which preceded the current research did not measure aerosol permeability until the shear wall had been loaded beyond its elastic limit to approximately 50 percent of the ACI 318-02 nominal capacity, and made only one series of measurements. They reported aerosol filtration efficiencies (AFE) ranging from 98.3 percent to 99.7 percent for a polydisperse spectrum of polystyrene latex (PSL) particles with diameters ranging from 0.065  $\mu\text{m}$  to 0.17  $\mu\text{m}$ .

After SFM testing was conducted, an aerosol was injected into the upstream chamber of the specimen and permitted to traverse the wall under steady-state flow for a period of several hours. Representative AFE spectra for each of four loading levels, computed using Equation (4), are shown in Figure 13. Aerosol testing at the  $0.30\phi V_n$  loading level was omitted due to practical limitations at the time of the test. Each spectrum was determined after comparable penetration time periods, ranging from 16 to 33 minutes. In this figure, two major facts are apparent. First, it is clear that aerosol penetration through the wall is quite low, even at the code design capacity. This indicates relative efficacy of such walls, within the limits of the testing conducted, as particulate barriers. Second, the scatter on the measurements can lead to apparently contradictory outcomes, such as the computed AFE for particles of 0.19  $\mu\text{m}$  diameter. For this diameter, it appears that filtration efficiency at the intermediate load levels is lower than at the undamaged and  $1.00\phi V_n$  states. The former condition is reasonable, but the latter is not. The results are biased by the absolute number of particles being measured. That is, the downstream chamber typically had measured particle concentrations on the order of  $10^5$  particles per in<sup>3</sup>, whereas the upstream chamber had concentrations on the order of  $10^7$  particles per in<sup>3</sup>. The dilution process needed to measure the upstream particle concentration causes slight variations in the number of particles counted to be amplified by the

dilution ratio, in this case  $D_r \approx 470$ . This means that a variation of  $10^3$  particles per  $\text{in}^3$  in the upstream measurement would be amplified to a variation of  $5 \times 10^5$  particles per  $\text{in}^3$ , or a 5 percent variation in the reported upstream concentration. This error would propagate when computing the AFE. The variability in the measurements means that all of the values may be statistically quite similar. Studies are underway at this time to quantify the actual error bounds on the AFE measurements.

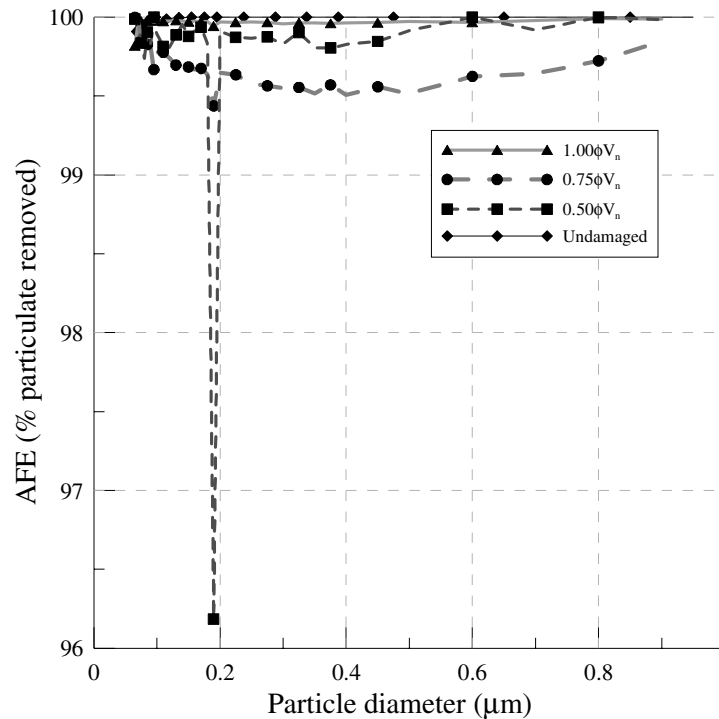


**Figure 13** Aerosol filtration efficiency (AFE) spectra for various loading levels

## CONCLUSIONS

Experiments were conducted to determine the correlation between containment efficacy degradation and induced damage for reinforced concrete shear walls. These tests consisted of in-plane loading of a shear wall under load control and subsequent measurement of gas permeability and aerosol filtration efficiency. A strong positive correlation was observed between increasing intrinsic permeability and increasing structural damage. Prior to application of the  $0.5\phi V_u$  load increment, intrinsic permeability remained essentially unchanged from its undamaged value, within one order of magnitude. After cycling at this load level, intrinsic permeability increased nearly linearly with increasing lateral load to a maximum of more than 400 times the undamaged value. Fintel's method for estimating permeability across undamaged concrete plates is accurate for these studies. Methods for predicting flow across cracked concrete members are evaluated in a companion paper [1]. Aerosol filtration efficiency remained high – 96 percent or greater – over the investigated spectrum of particle diameters, despite increasing structural damage. Aerosol particle count variability may impact the reliability of AFE measurements, and studies are underway to quantify the extent of this variability. No models are available in the literature to predict aerosol filtration efficiency. This ongoing research program, in combination with prior tests by Farrar and Girrens, will support the future development of such models. It must be stressed that the specimen

geometry and material properties can reasonably be expected to strongly influence the relationship between structural damage and containment efficacy, so the experimental results presented herein must be applied only with great caution to facilities with other configurations.

### ACKNOWLEDGMENTS

This research was funded by the Los Alamos National Laboratory under Contract 33337-001-01-49. The Henry Samueli School of Engineering Alumni Scholarship provided partial support for the last author. Their support is gratefully acknowledged.

### REFERENCES

1. Wang, T, Hutchinson, TC, Hamilton, CH, Pardoen, GC, Salmon, MW. "Gas leakage rate through reinforced concrete shear walls: Numerical study." *Proceedings of the 13<sup>th</sup> World Conference on Earthquake Engineering*, Vancouver, BC, Canada. Paper no. 34.
2. ACI. *Building code requirements for structural concrete* (ACI 318-02) and commentary (ACI 318R-02), Farmington Hills, MI: American Concrete Institute, 2002.
3. Girrens, SP, Farrar, CR. *Experimental assessment of air permeability in a concrete shear wall subjected to simulated seismic loading*, Report LA-12124-MS, Los Alamos, New Mexico: Los Alamos National Laboratory, July, 1991.
4. Fintel, M, Editor. *Handbook of concrete engineering*. New York, New York. Van Nostrand Reinhold. 1974.
5. Figg, JW. "Method of measuring the air permeability of concrete." *Magazine of Concrete Research* 1973; 25(85): 213-218.
6. Farrar, CR, Girrens, SP. *Aerosol penetration through a seismically loaded shear wall*. Report LA-UR 92-590. Los Alamos, New Mexico: Los Alamos National Laboratory, June, 1992.